RSC Advances

PAPER

View Article Online
View Journal | View Issue

Cite this: *RSC Adv.*, 2020, **10**, 18583

Fluoxetine scaffold to design tandem molecular antioxidants and green catalysts†

Giovanni Ribaudo, [a] Marco Bortoli, [b] Alberto Ongaro, [a] Erika Oselladore, [c] Alessandra Gianoncelli, [a] Giuseppe Zagotto [c] and Laura Orian [*b]

Received 19th April 2020
Accepted 7th May 2020

DOI: 10.1039/d0ra03509b

rsc.li/rsc-advances

Fluoxetine finds application in the treatment of depression and mood disorders. This selective serotonin-reuptake inhibitor (SSRI) also contrasts oxidative stress by direct ROS scavenging, modulation of the endogenous antioxidant defense system, and/or enhancement of the serotonin antioxidant capacity. We synthesised some fluoxetine analogues incorporating a selenium nucleus, thus expanding its antioxidant potential by enabling a hydroperoxides-inactivating, glutathione peroxidase (GPx)-like activity. Radical scavenging and peroxidatic activity were combined in a water-soluble, drug-like, tandem antioxidant molecule. Selenofluoxetine derivatives were reacted with H_2O_2 in water, and the mechanistic details of the reaction were unravelled combining nuclear magnetic resonance (NMR), electrospray ionisation-mass spectrometry (ESI-MS) and quantum chemistry calculations. The observed oxidation–elimination process led to the formation of seleninic acid and cinnamylamine in a *trans*-selective manner. This mechanism is likely to be extended to other substrates for the preparation of unsaturated cinnamylamines.

Introduction

Fluoxetine hydrochloride (*N*-methyl-3-phenyl-3-[4-(trifluoromethyl)phenoxy]propan-1-amine HCl) is a selective serotonin-reuptake inhibitor (SSRI), which was approved by the FDA in 1987 for the treatment of depression.[1,2] This drug, marketed as Prozac by Eli Lilly, enhances the serotoninergic tone by increasing the concentration of the neurotransmitter in the synaptic cleft by inhibiting the serotonin transporter.[3] From a structural point of view, it is constituted by a racemic mixture of *R*(−)-fluoxetine and *S*(+)-fluoxetine, which show a moderate difference in terms of inhibitory activity that becomes more evident in the corresponding metabolites.[4] Fluoxetine has been approved worldwide for the treatment of major depression, but its activity on a wide spectrum of mood disorders has been reported.[5]

Further studies unveiled that fluoxetine may protect against the adverse effects of different types of immune system stressors and contrast, through a combination of mechanisms, oxidative damage. This feature is thought to play a primary role in neuroprotection, since brain is very susceptible to oxidative stress due to its high energetic requirement. Moreover, growing evidence suggests that oxidative stress and an abnormally increased generation of reactive oxygen species (ROS) may be implicated in the pathogenesis of many psychiatric and degenerative disorders.[6–10] Considering the mechanistic aspects, the insurgence of such diseases may be the result of ROS-related damage, *i.e.* lipid peroxidation, DNA or protein oxidation, and mitochondrial damage. From a biochemical and clinical point of view, the antioxidant effects of antidepressant agents were observed in animal models by measuring variations of GSH, malondialdehyde, nitric oxide and isoprostanes concentrations.[11–13]

At molecular level, it has been highlighted that fluoxetine exerts its antioxidant effects through a combination of mechanisms, involving direct ROS scavenging, modulation of the expression and functioning of enzymatic and non-enzymatic components of the endogenous antioxidant defence system, and/or enhancement of the serotonin antioxidant capacity.[14,15] Concerning the first putative mechanism, the activity of fluoxetine against ROS has been thoroughly studied from a biochemical and computational point of view. Although the compound demonstrated an antioxidant role, its direct contribution to ROS scavenging is of a minor entity with respect to that of its metabolites.[16,17] In addition, fluoxetine contrasts oxidative stress also by increasing extracellular concentration of serotonin, which is a known strong antioxidant.[17–19] This neurotransmitter, together with its *N*-acetyl metabolite, exerts neuroprotection by modulating oxidative burst mechanism and/or the production of superoxide anion radical.[19] Fluoxetine is also thought to act indirectly on oxidative stress by modulating the expression of enzymes such as superoxide dismutase

[a]*Dipartimento di Medicina Molecolare e Traslazionale, Università degli Studi di Brescia, Viale Europa 11, 25123 Brescia, Italy*

[b]*Dipartimento di Scienze Chimiche, Università degli Studi di Padova, Via Marzolo 1, 35131 Padova, Italy. E-mail: laura.orian@unipd.it*

[c]*Dipartimento di Scienze del Farmaco, Università degli Studi di Padova, Via Marzolo 5, 35131 Padova, Italy*

† Electronic supplementary information (ESI) available. See DOI: 10.1039/d0ra03509b

(SOD), catalase (CAT) and glutathione peroxidase (GPx).[14] Finally, recent findings suggest that fluoxetine may enhance cellular antioxidant capacity by tuning mitochondrial redox parameters and through the upregulation of thioredoxin (Trx), a dithiol-disulfide oxidoreductase that can facilitate H_2O_2 scavenging.[20] Nevertheless, the indirect antioxidant role that fluoxetine plays in neuroprotection is still debated. Particularly, Dalmizrak *et al.* reported that long-term use of fluoxetine may be connected with glutathione reductase (GR) deficiency,[21] while Byeon *et al.* pointed out that SSRIs might mediate oxidative stress in aquatic invertebrates.[22]

In the above described scenario, we have synthesised chimeric derivatives of fluoxetine that have been modified to incorporate a selenium nucleus, thus providing an additional mechanism to enhance its molecular antioxidant performance (Fig. 1).

Besides the radical scavenging activity *via* HAT (Hydrogen Atom Transfer) mechanism, recently reported for fluoxetine,[17] selenofluoxetine and its derivatives have the capacity of reducing hydroperoxides and H_2O_2 as GPx mimics.[23–25] The biological role of selenium is a long-debated issue since its identification in GPx, an enzyme able to protect cells from oxidative stress by inactivating hydroperoxides.[26–30] As often happens, nature inspired medicinal chemists and synthetic selenium-based compounds were developed through the years to mimic GPx activity as well as to exert antioxidant activity through other mechanisms, such as metal binding.[23–25,31] Among GPx mimics, ebselen (2-phenyl-1,2-benzisoselenazol-3(2*H*)-one) is the most popular since it was employed in clinical trials.[32] Aryl and alkyl selenides,[33,34] together with aryl diselenides,[35–38] have been prepared and tested *in vitro* and *in vivo*. In addition, unsubstituted alkylphenyl selenides and diphenyldiselenide have been adopted to study the reactivity towards peroxides as models for understanding the behaviour of organoselenides in biological environments.[39] Since selenides are largely used in organic synthesis to catalyze oxidation in presence of H_2O_2, combined experimental and theoretical mechanistic studies on model organoselenides are important also for designing selenium based organocatalysts.[40–45]

The rationale that guided the design of the selenium-containing analogues of fluoxetine aims to combine the antioxidant radical scavenging capacity, within the CNS, of the parent compound with the GPx-like activity of organic selenides in a water-soluble drug-like small molecule (*tandem antioxidant*). Thus, selenofluoxetine and its derivatives here reported represent models for the experimental and theoretical investigation of their elementary, but biologically as well as chemically significant, reaction with H_2O_2. As will be discussed in the following, the oxidation–elimination process observed for the studied compounds leads to the production of a cinnamylamine. Such scaffold is found in many drugs like flunarizine (calcium antagonist) and naftifine (antifungal). It must be noted that other strategies for the synthesis of allylamines were previously reported in the literature, such as the preparation from alcohols and amines through alkoxyphosphonium salts,[46] the reduction of secondary amides followed by *N*-methylation[47] or the reduction of propargylamines.[48] Nevertheless, the cited methods require hazardous and expensive reactants, harsh experimental conditions (temperature and pressure) and do not guarantee stereoselectivity. By contrast, the approach we propose efficiently proceeds in aqueous medium, it is *trans*-selective and requires only H_2O_2 as oxidant agent. Nuclear magnetic resonance (NMR) and electrospray ionisation-mass spectrometry (ESI-MS) combined with quantum chemistry calculations are used to characterise intermediates and products and to draw energy profiles based on which the mechanistic details are unravelled.

Experimental

Chemistry

Commercially available chemicals were purchased from Sigma-Aldrich and used without any further purification if not specified elsewhere. NMR experiments were performed on a Bruker Avance III 400 spectrometer (frequencies: 400.13, 100.62, and 76.37 MHz for ^{1}H, ^{13}C, and ^{77}Se nuclei, respectively) equipped with a multinuclear inverse z-field gradient probe head (5 mm). For data processing, TopSpin 4.0.8 software was used and the spectra were calibrated using solvent signal (^{1}H-NMR, δ_H = 7.26 ppm for $CDCl_3$, $\delta_H = 2.50$ ppm for DMSO-d_6, $\delta_H = 4.79$ ppm for D_2O; ^{13}C-NMR, $\delta_C = 77.16$ ppm for $CDCl_3$, $\delta_C = 39.52$ ppm for DMSO). Multiplicities are reported as follows: s, singlet; d, doublet; t, triplet; q, quartet; m, multiplet; b, broad; dd, doublet of doublets. Mass spectra were recorded by direct infusion ESI on a Thermo Fisher Scientific LCQ Fleet ion trap mass spectrometer and on a Waters Xevo G2 QTof high-resolution mass spectrometer (HRMS). The purity profile of the compounds was assayed by HPLC using a Varian Pro-Star system equipped with a Biorad 1706 UV-VIS detector and an Agilent C-18 column (5 μm, 4.6 × 150 mm). An appropriate ratio of water (A) and acetonitrile (B) was used as mobile phase with an overall flow rate of 1 mL min^{-1}. The general method for the analyses is

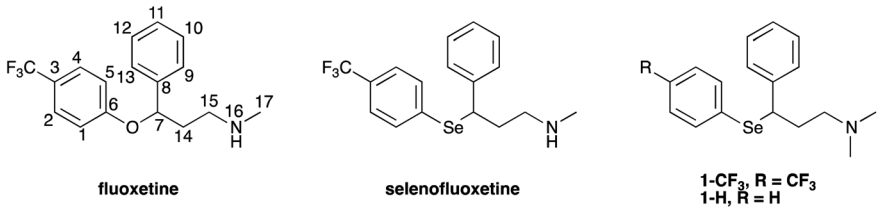

Fig. 1 Fluoxetine and its derivatives studied in this work.

reported here: 0 min (90% A–10% B), 5 min (90% A–10% B), 25 min (10% A–90% B), 30 min (90% A–10% B), and 32 min (90% A–10% B). The purity of all compounds was ≥96%, unless otherwise stated (254 nm).

Synthesis of *N*,*N*-dimethyl-3-oxo-3-phenylpropan-1-aminium chloride (2). Dimethylamine hydrochloride (2.03 g, 24.9 mmol, 1.5 eq.) and paraformaldehyde (0.65 g, 21.6 mmol, 1.3 eq.) were weighted in a 50 mL round-bottomed flask and dissolved in 2.5 mL of ethanol. Acetophenone (2.00 g, 16.6 mmol, 1 eq.) was added to the solution together with 40 μL of concentrated hydrochloric acid. The reaction mixture was stirred at reflux and checked through TLC (DCM/MeOH/TEA 97 : 2.5 : 0.5). After 2 hours, the solution was left to cool to room temperature. A solid precipitate of *N*,*N*-dimethyl-3-oxo-3-phenylpropan-1-aminium chloride salt formed and the solid was filtered with a Buchner funnel, washed with cold acetone (3 × 10 mL) and with hexane (1 × 10 mL). Yield 3.48 g (98%); white solid; ^{1}H-NMR (400 MHz, DMSO): δ_H (ppm) 10.57 (br, 1H, N*H*), 8.02 (d, 2H, J = 7.2 Hz, Ph-*H*), 7.69 (t, 1H, J = 7.4 Hz, Ph-*H*), 7.57 (t, 2H, J = 7.6 Hz, Ph-*H*), 3.63 (t, 2H, J = 7.2 Hz, C(O)CH_2), 3.40 (t, 2H, J = 7.2 Hz, CH_2N), 2.80 (s, 6H, N(CH_3)$_2$); ^{13}C-NMR (101 MHz, DMSO): δ_C (ppm) 196.8 (s, *C*(O)), 135.9 (s, Ph-*C*), 133.7 (s, 2C, Ph-*C*), 128.8 (s, Ph-*C*), 128.0 (s, 2C, Ph-*C*), 51.8 (s, *C*H$_2$N), 42.2 (s, 2C, N(*C*H$_3$)$_2$), 33.1 (s, C(O)*C*H$_2$); (HRMS ESI$^+$) m/z calcd for $C_{11}H_{16}NO^+$ [M + H]$^+$: 178.1232; found: 178.1308.

Synthesis of 3-hydroxy-*N*,*N*-dimethyl-3-phenylpropan-1-amine (3). Compound **2** (1.80 g, 8.39 mmol, 1 eq.) was dissolved in 5 mL of distilled water and 1.2 mL of a solution 8 M of KOH was added to the mixture. A white solid precipitate formed and the mixture was extracted with DCM (4 × 20 mL). The organic phases were combined, and the solvent was evaporated under reduced pressure, yielding the free base of compound **2**. The oily compound was dissolved in 10 mL of methanol and a couple of drops of KOH 8 M were added in order to provide an alkaline environment. The solution was cooled to 0 °C with an ice bath and sodium borohydride (0.47 g, 12.6 mmol, 3 eq.) was added to the solution. When all the reactants were dissolved, the ice bath was removed and the mixture was stirred at room temperature for 1.5 hours. After said time, concentrated hydrochloric acid was added dropwise to the solution until acid pH, then the solution was again basified with KOH 8 M. The methanol was evaporated under reduced pressure and the precipitate was dissolved in 100 mL of DCM and washed with alkaline water (4 × 10 mL). The organic phase was dried with anhydrous magnesium sulphate and filtered, then the solvent was evaporated under reduced pressure. Yield 1.43 g (95%); transparent oil; ^{1}H-NMR (400 MHz, $CDCl_3$): δ_H (ppm) 7.41–7.31 (m, 4H, Ph-*H*), 7.28–7.22 (m, 1H, Ph-*H*), 4.91 (dd, J = 7.1, 4.7 Hz, 1H, C*H*(OH)), 2.66–2.58 (m, 1H, CH(OH)CH_AH_B), 2.48–2.42 (m, 1H, CH(OH)CH$_A$*H*$_B$), 2.28 (s, 6H, N(CH_3)$_2$), δ_H 1.86–1.79 (m, 2H, CH_2N); ^{13}C-NMR (101 MHz, $CDCl_3$): δ_C (ppm) 145.1 (s, Ph-*C*), 128.1 (s, 2C, Ph-*C*), 126.8 (s, Ph-*C*), 125.5 (s, 2C, Ph-*C*), 75.3 (s, *C*H(OH)), 58.1 (s, *C*H$_2$N), 45.2 (s, 2C, N(*C*H$_3$)$_2$), 34.7 (s, CH(OH)*C*H$_2$); (HRMS ESI$^+$) m/z calcd for $C_{11}H_{18}NO^+$ [M + H]$^+$: 180.1383, found: 180.1133.

Synthesis of 3-chloro-*N*,*N*-dimethyl-3-phenylpropan-1-aminium chloride (4). Compound **3** (1.50 g, 8.37 mmol) was dissolved in a small amount of diethyl ether and 5 mL of HCl 2 M in ether were added in order to obtain the hydrochloride salt. The solvent was evaporated under reduced pressure. 10 mL of thionyl chloride were added to the round-bottomed flask and the solution was stirred under reflux. The reaction was followed through TLC (DCM/MeOH/TEA 97 : 2.5 : 0.5) and was stopped after 2 hours when the starting material spot was no longer detected. The solvent was evaporated under reduced pressure obtaining the compound as hydrochloride salt. Yield 1.88 g (96%), white solid; ^{1}H NMR (400 MHz, DMSO): δ_H (ppm) 10.90 (br, 1H, N*H*), 7.52–7.49 (m, 2H, Ph-*H*), 7.45–7.35 (m, 3H, Ph-*H*), 5.31 (dd, J = 9.1, 5.2 Hz, 1H, C*H*(Cl)), 3.23–3.18 (m, 1H, CH(Cl)CH_AH_B), 3.10–3.04 (m, 1H, CH(Cl)CH$_A$*H*$_B$), 2.76 (s, 6H, N(CH_3)$_2$), 2.63–2.44 (m, 2H, CH_2N); ^{13}C-NMR (101 MHz, DMSO): δ_C (ppm) 141.0 (s, Ph-*C*), 129.3 (s, 2C, Ph-*C*), 129.2 (s, 2C, Ph-*C*), 127.5 (s, Ph-*C*), 61.1 (s, *C*H(Cl)), 42.7 (s, *C*H$_2$N), 42.4 (s, 2C, N(*C*H$_3$)$_2$), 33.6 (s, CH(Cl)*C*H$_2$); (HRMS ESI$^+$) m/z calcd for $C_{11}H_{17}ClN^+$ [M + H]$^+$: 198.1044, found: 198.1043.

Synthesis of 1,2-bis(4-(trifluoromethyl)phenyl)diselane (5). Under nitrogen atmosphere, magnesium chips (108 mg, 4.44 mmol, 1 eq.) were added to a solution of 4-bromobenzotrifluoride (1.00 g, 4.44 mmol, 1 eq.) in dry ether in a 50 mL three-necked round-bottomed flask. The halobenzene solution was added dropwise at gentle reflux and left stirring for another 30 minutes. Afterwards selenium powder (351 mg, 4.44 mmol, 1 eq.) was added maintaining gentle refluxing and the reaction mixture was stirred for another 30 minutes. Then the mixture was poured in a mixture of cracked ice and concentrated hydrochloric acid. The cold mixture was separated and the water phase was extracted with ether (3 × 20 mL). The combined organic layer was dried over anhydrous magnesium sulphate, which was then removed by filtration. The solvent was removed under reduced pressure. Yield 1.21 g (61%); orange oil; ^{1}H-NMR (400 MHz, $CDCl_3$): δ_H (ppm) 7.71 (d, J = 8.0 Hz, 4H, Ph-*H*), 7.52 (d, J = 8.2 Hz, 4H, Ph-*H*); ^{13}C-NMR (101 MHz, $CDCl_3$): δ_C (ppm) 135.0 (s, 2C, Ph-*C*), 130.9 (s, 4C, Ph-*C*), 129.9 (q, J = 28.9 Hz, 2C, Ph-*C*), 126.2 (q, J = 3.7 Hz, 4C, Ph-*C*), 123.4 (q, J = 328.1 Hz, 2C, *C*F$_3$). (ESI$^+$) m/z calcd for $C_{14}H_9F_5Se_2^+$ [M–F + H]$^+$:431.89, found: 431.44.

Synthesis of *N*,*N*-dimethyl-3-phenyl-3-((4-(trifluoromethyl)phenyl)selanyl)propan-1-amine (1-CF$_3$). The diselenide **5** (373 mg, 0.85 mmol, 1 eq.) was introduced in a 50 mL round-bottomed flask and dissolved in ethanol, KOH (143 mg, 2.55 mmol, 3 eq.) was added and the solution was cooled in an ice bath. Then, sodium borohydride (193 mg, 5.10 mmol, 6 eq.) was added. Once that a colour change was observed (between 30 minutes and 1 hour after the reaction began), compound **4** (200 mg, 0.85 mmol, 1 eq.) was added to the solution. The reaction was stirred at room temperature for 3 hours. To quench the unreacted $NaBH_4$, concentrated hydrochloric acid was added to the mixture until acidic pH. Afterwards KOH 8 M was added to basic pH. Ethanol was evaporated under reduced pressure and the precipitate that formed was dissolved in DCM. The solution was washed with alkaline water (3 × 20 mL), dried over anhydrous magnesium sulphate and filtered, then the solvent was evaporated under reduced pressure. The product was purified by column chromatography (silica gel, DCM/

MeOH/TEA, 92 : 7.5 : 0.5). Yield 112 mg (34%); yellow oil; ^{1}H-NMR (400 MHz, $CDCl_3$): δ_H (ppm) 7.49 (d, J = 8.0 Hz, 2H, Ph-*H*), 7.43 (d, J = 8.4 Hz, 2H, Ph-*H*), 7.29–7.19 (m, 5H, Ph-*H*), 4.49–4.46 (m, 1H, C*H*(Se)), 2.38–2.22 (m, 4H, CHCH_2CH_2N), 2.22 (s, 6H, N(CH_3)$_2$); ^{13}C-NMR (101 MHz, $CDCl_3$): δ_C (ppm) 141.72 (s, Ph-*C*), 134.9 (s, 2C, Ph-*C*), 134.7 (s, Ph-*C*), 129.7 (q, J = 32.6 Hz, Ph-*C*), 128.6 (s, 2C, Ph-*C*), 127.9 (s, 2C, Ph-*C*), 127.4 (s, Ph-*C*), 125.6 (q, J = 3.7 Hz, 2C, Ph-*C*), 124.2 (q, J = 272.19 Hz, *C*F_3), 57.8 (s, *C*H(Se)), 46.3 (s, CH_2N), 45.4 (s, 2C, N(CH_3)$_2$), 34.0 (s, CH(Se)*C*H_2); (HRMS ESI$^+$) m/z calcd for $C_{18}H_{21}F_3NSe^+$ [M + H]$^+$: 388.0786, found: 388.0866.

Synthesis of *N*,*N*-dimethyl-3-phenyl-3-(phenylselanyl) propan-1-amine (1-H). The diphenyl diselenide (400 mg, 1.28 mmol, 1 eq.) was introduced in a 50 mL round-bottomed flask and dissolved in ethanol, KOH (215 mg, 3.84 mmol, 3 eq.) was added and the solution was cooled in an ice bath. Then, sodium borohydride (290 mg, 7.68 mmol, 6 eq.) was added. Once that a colour change was observed (between 30 minutes and 1 hour after the reaction began), compound **4** (300 mg, 1.28 mmol, 1 eq.) was added to the solution. The reaction was stirred at room temperature for 3 hours. To quench the unreacted $NaBH_4$, concentrated hydrochloric acid was added to the mixture until acidic pH. Afterwards KOH 8 M was added to basic pH. The solvent was evaporated under reduced pressure and the precipitate that formed was dissolved in DCM. The solution was washed with alkaline water (3 × 20 mL), dried over anhydrous magnesium sulphate and filtered, then the solvent was evaporated under reduced pressure. The product was purified by column chromatography (silica gel, DCM/MeOH/TEA, 92 : 7.5 : 0.5). Yield 155 mg (38%); yellow oil; ^{1}H-NMR (400 MHz, $CDCl_3$): δ_H (ppm) 7.43–7.40 (m, 2H, Ph-*H*), 7.28–7.18 (m, 8H, Ph-*H*), 4.38–4.33 (m, 1H, C*H*(Se)), 2.31–2.19 (m, 4H, CH(Se)CH_2CH_2N), 2.17 (s, 6H, N(CH_3)$_2$); ^{13}C-NMR (101 MHz, MeOD): δ_C (ppm) 140.6 (s, Ph-*C*), 135.5 (s, Ph-*C*), 128.8 (s, 2C, Ph-*C*), 128.4 (s, Ph-*C*), 128.3 (s, 2C, Ph-*C*), 128.0 (s, 2C, Ph-*C*), 127.3 (s, Ph-*C*), 127.2 (s, 2C, Ph-*C*), 56.4 (s, *C*H(Se)), 43.7 (s. CH_2N), 42.1 (c, 2C, N(*C*H_3)$_2$), 30.5 (s, CH(Se)*C*H_2); (HRMS ESI$^+$) m/z calcd for $C_{17}H_{22}NSe^+$ [M + H]$^+$: 320.0912, found: 320.1072.

NMR study of the reaction with H_2O_2

In order to study the oxidation reaction of compounds **1-CF$_3$** and **1-H**, their reaction with H_2O_2 was investigated by ^{1}H-NMR in an aqueous environment at room temperature (22 °C). The compounds were used as hydrochloride salts (28 mM: **1-CF$_3$** = 4.9 mg, 11.6 μmol and **1-H** = 5.6 mg, 17.6 μmol) and dissolved in D_2O, t_0 spectra were registered with 8 scans, 1 dummy scan and a delay time d_1 of 2 s. Afterwards, H_2O_2 (1.1 eq., H_2O_2 3% w/w solution: **1-CF$_3$** = 15 μL, **1-H** = 18 μL) was added and the spectra were registered every 2 or 5 minutes until the reaction was complete (47 min for **1-CF$_3$** and 104 min for **1-H**) (8 scans, 1 dummy scan, d_1 of 2 s). The reaction was studied plotting the results of the integration of the signals corresponding to the protons bound to the carbon adjacent to the selenium atom for the starting material, and the two diastereoisomers and the allylic hydrogens for the cinnamylamine. ^{1}H–^{77}Se HMBC NMR spectra were acquired using a repetition delay of 1 s; a total of 300 experiments of 16–40 scans were accumulated and processed with a magnitude calculation; an evolution delay of 33.3 ms was used for ^{1}H–^{77}Se long-range coupling constants; the spectral width was 13 ppm in F_2 and 1000 ppm in F_1. Zero-filling in the F_1 and F_2 dimensions, multiplication with a Gaussian function (in F_2) and a squared sine function (in F_1) were performed prior to 2D Fourier transformation.

ESI-MS study of the reaction with H_2O_2

Mechanistic ESI-MS studies were performed under the same experimental conditions (concentration and temperature) used in the NMR analysis, except for the fact that Milli-Q water was used instead of D_2O. Solutions were diluted 1 : 1000 in methanol before the analysis. Spectra were recorded by direct infusion ESI on a Thermo Fisher Scientific (Waltham, MA) LCQ Fleet ion trap mass spectrometer. ESI parameter for positive ionisation mode are here described: 4.0 kV spray voltage, 225 °C capillary temperature, 5 μL min^{-1} flow rate. For negative ionisation mode: 5.0 kV spray voltage, 180 °C capillary temperature, 5 μL min^{-1} flow rate.

Computational methodology

For hydrogen atom transfer (HAT) reactions, geometry optimisations of the reactants and products were performed in the gas phase without any constraint, using the M06-2X functional[49] combined with the 6-31G(d) basis set, as implemented in Gaussian 16.[50] Spin contamination was checked for the doublet ground state species to assess the reliability of the wavefunction. To confirm the nature of the stationary points and to obtain the thermodynamic corrections at 1 atm and 298 K, frequency calculations at the M06-2X/6-31G(d) level of theory were run to ascertain that only positive frequencies were present. In order to obtain more accurate energy values, single-point energy calculations were performed at M06-2X/6-311+G(d,p) in the gas phase, and subsequently, at the same level of theory, in benzene and water using the continuum Solvation Model based on Density (SMD).[51] This level of theory is denoted in the text (SMD)-M06-2X/6-311+G(d,p)//M06-2X/6-31G(d,p). The choice fell on benzene and water because the model an apolar and a polar environment, respectively.[52] Energy barriers were calculated for the most reactive sites (identified on the basis of ΔG°_{HAT}), at the (SMD)-M06-2X/6-311+G(d,p)//M06-2X/6-31G(d,p) level of theory. Analysis of the single imaginary frequency of transition states confirmed that the normal mode involved was correct for the HAT process. Energy barriers were calculated, referring to the free reactants in the gas phase as well as in the solvent.

The quantum chemistry calculations for the Se oxidation mechanism were performed using the Amsterdam Density Functional (ADF).[53–55] The energy profiles were obtained from geometries and energies computed by using the OLYP functional,[56,57] which is known to perform well for reactivity studies on organic compounds, and it has been recently benchmarked[58] and applied[59] to organic dichalcogenides. OLYP was combined with the TZ2P basis set for all the atoms.[60] The TZ2P basis set is of triple-ζ quality and has been augmented with two sets of

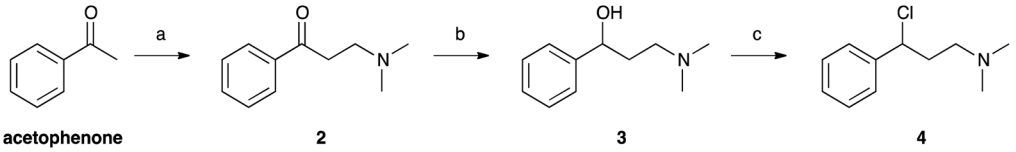

Scheme 1 (a) dimethylamine HCl/HCOH/EtOH; (b) $NaBH_4$/KOH/MeOH; (c) $SOCl_2$.

polarisation functions. Core shells of the atoms (1s for C, F, N and O and up to 3p for Se) were treated by using the frozen-core approximation. Scalar relativistic effects were treated using the Zeroth Order Regular Approximation (ZORA).[61–63] The numerical integration was performed by using the fuzzy-cell integration scheme developed by Becke.[64,65] Energy minima and transition states have been verified through vibrational analysis. All minima were found to have zero imaginary frequencies and all transition states have one that correspond to the mode of the reaction under consideration. For single point calculations in water the conductor-like screening Model was employed (COSMO), as implemented in ADF.[66–68] Water was parameterised using a dielectric constant of 78.39 and a solvent radius of 1.93 Å.

Results and discussion

Synthesis of the selenium-based fluoxetine analogues

Selenofluoxetine closely resembles fluoxetine, in which oxygen was substituted with a selenium atom. *N*,*N*-dimethyl derivatives **1-CF$_3$** and **1-H** (Fig. 1) were designed to simplify synthetic procedures and were used for the experimental reactivity studies. Compounds **1-CF$_3$** and **1-H**, were obtained through a multi-step synthesis. Acetophenone was initially subjected to a *Mannich* reaction with dimethylamine hydrochloride and formaldehyde giving compound **2**.[69] The *Mannich* base was then reduced with sodium borohydride providing compound **3** as two enantiomers,[70] and subsequently chlorinated with thionyl chloride obtaining the intermediate synthon **4** (Scheme 1).[71]

The chloride was then displaced by the appropriate selenide nucleophile, formed *in situ* by the reduction of the corresponding diphenyl diselenide with sodium borohydride, providing **1-CF$_3$** and **1-H** (Scheme 2; please refer to ESI† for detailed experimental procedures and analytical data). Particularly, 1,2-bis(4-(trifluoromethyl)phenyl)diselane (compound **5**) was obtained through the reaction with elemental selenium of the *Grignard* reagent formed from *p*-trifluoromethyl bromobenzene (see Fig. S1–S22† for ^{1}H, ^{13}C and mass spectra).[72,73] The unsubstituted diphenyl diselenide is commercially available.

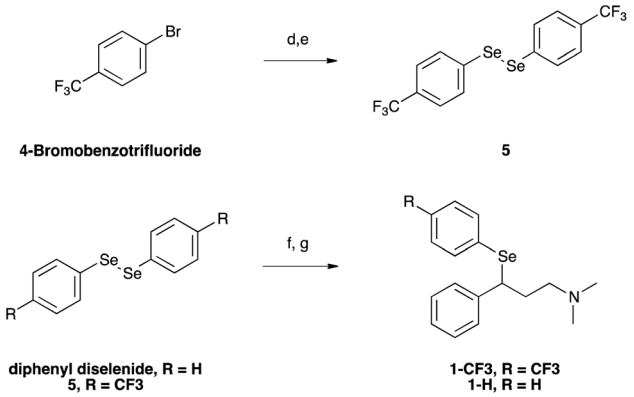

Scheme 2 (d) Mg/Et_2O; (e), Se; (f) $NaBH_4$/KOH/EtOH; (g) compound **3**/EtOH.

Oxidation by H_2O_2: NMR results

In our experimental model reaction, the process initiates upon addition of H_2O_2 and evolves to an oxidation-triggered elimination, which is peculiar of selenides having protons in the β-position with respect to the chalcogen nucleus (Scheme 3). It is a highly *trans*-selective process affording olefins, and it was demonstrated that it occurs through a *syn* mechanism.[74]

The first step of the process consists in the oxidation of the starting selenide to the corresponding selenoxide. It has been reported that this reaction can occur using hydrogen peroxide (H_2O_2), *meta*-chloroperoxybenzoic acid (*m*CPBA) and ozone.[39,75,76] This process promotes the formation of a new chiral centre, giving rise to two enantiomers or to two diastereoisomers, depending on the initial compound. Then, an intramolecular *syn* elimination takes place: a proton is transferred from the β-position to the oxygen of the selenoxide, and the selenium–carbon bond breaks leading to the formation of a carbon–carbon double bond (Scheme 4).[77]

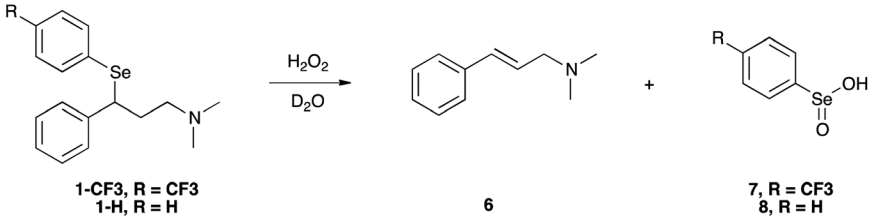

Scheme 3 Oxidation of **1-CF$_3$** and **1-H** by H_2O_2. This scheme represents the overall reaction leading to the formation of cinnamylamine and seleninic acid, which were experimentally observed as final products.

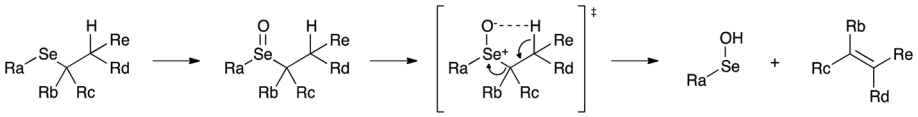

Scheme 4 Mechanistic details of selenoxide elimination leading to the formation of selenenic acid and olefin. Selenenic acid undergoes disproportionation and only seleninic acid was experimentally observed.

The above described selenoxide elimination was studied considering the selenium-based analogues of fluoxetine as models. As anticipated, fluoxetine was modified with the aim of improving its antioxidant properties through the substitution of its oxygen atom with selenium, leading to compound **1-CF$_3$**. In this connection, compound **1-H** was designed as a further simplified model for our investigation aiming at drawing widely general conclusions. Finally, due to synthetic feasibility and to improve water solubility, both analogues differ from fluoxetine also for the presence of a tertiary amine instead of a secondary amine. To explore the potential application of these derivatives in the field of green chemistry and to better mimic a biologically relevant environment, the oxidation of **1-H** was performed in water. Indeed, although selenium and its oxidised species were reported to show toxic effect at high concentrations,[78] growing attention is recently being paid to organoselenides catalysing organic reactions in environmentally friendly conditions.[79] In particular, this holds true when aqueous medium is considered.[80] In this context, good water solubility was achieved for **1-H** and **1-CF$_3$**, since the compounds were prepared as hydrochloride salts. Firstly, to gain insight into the reaction mechanism and to fully characterise intermediates and products, the whole process was followed by ^{1}H-NMR spectroscopy according to the procedure reported in the Experimental section. Compounds were dissolved in deuterated water and the oxidation was carried out at room temperature using 1 equivalent of H_2O_2. During the reaction of **1-H**, prompt disappearance of the signal corresponding to the α position proton of the starting material (4.42 ppm) occurred, accompanied by the appearance of the signals of the two selenoxide diastereoisomers (4.48 ppm and 4.23 ppm) (Fig. 2). The same behaviour was observed for **1-CF$_3$**, but the signal of one of the two selenoxide diastereoisomers unluckily overlap to the signals of the starting material (approximately 4.55 ppm), thus complicating the mechanistic investigation (Fig. S23–S25†).

When a chiral centre is present in the starting compound, since in the transition state the carbon–hydrogen and carbon–selenium bonds are co-planar, the two selenoxide diastereoisomer products may react with different formation and subsequent different elimination rate (Fig. 2). This phenomenon will be discussed more in detail in the computational section, since even slight differences in the activation energies for the elimination reactions that are strictly related to the structure of the transition states may affect the reaction speed.

As the reaction proceeded, it was possible to observe the disappearance of the selenoxide diastereoisomers (depicted in Fig. 2(a)) and the formation of the elimination products: (*E*)-*N*,*N*-dimethyl-cinnamyl amine **6**, which was characterised by NMR, and the corresponding highly oxidised Se-containing species, *i.e.* seleninic acids **7** and **8**. At this stage, it must be noted that seleninic acid itself is endowed with synthetic value in the context of organic catalysis. It is indeed generally referred to as a pre-catalyst,[81] which can be converted to the corresponding benzeneperoxyseleninic acid, a known oxygen-transfer agent, in presence of an excess of peroxide.[82,83] For the studied compounds, the overall reaction demonstrated to

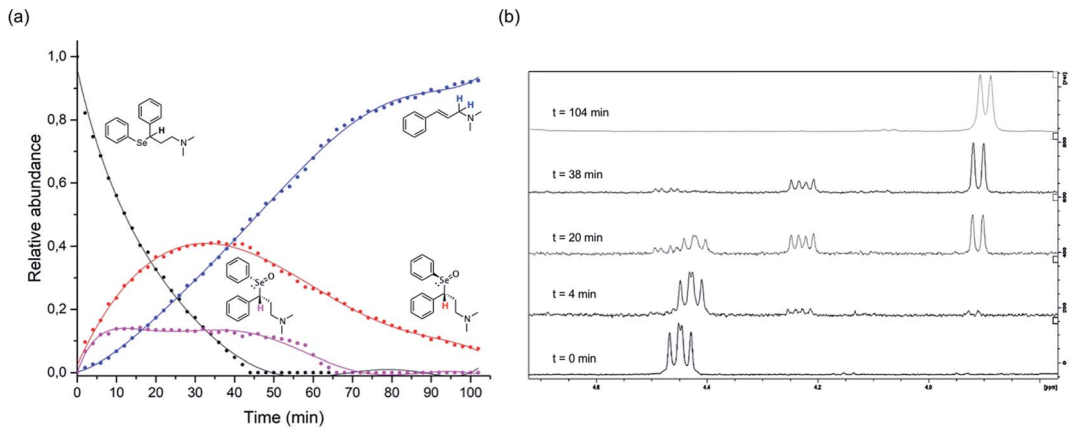

Fig. 2 ^{1}H-NMR mechanistic study of the reaction of **1-H** with H_2O_2. The graph reported in (a) was obtained by integration of the α-hydrogen signals for the starting material and the two diastereoisomers and the allylic-hydrogens signals for the cinnamylamine in the ^{1}H-NMR spectra acquired at different time points (• starting material, • *R*–*R* (and its enantiomer), • *R*–*S* (and its enantiomer) • cinnamylamine **6**). In (b), representative ^{1}H-NMR spectra are reported showing the variation over time during the oxidation-reaction of compound **3**, focusing on the region between 4.7 and 3.8 ppm (area of interest to plot the graph; see Fig. S31† for additional spectra).

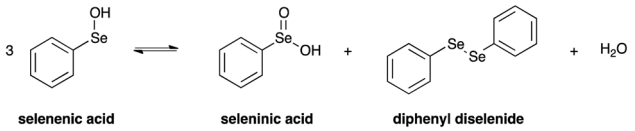

Scheme 5 Redox equilibrium involving differently oxidised selenium species.

be relatively fast. Particularly, a 90% conversion was observed for **1-CF$_3$** after 36 minutes, whereas for **1-H** the same conversion was achieved after 95 minutes (Fig. S26† and 2).

Importantly, it has to be pointed out that selenenic acid is involved in the chemical equilibrium reported in Scheme 5,[77] and according to this mechanism it disproportionates providing seleninic acid, diphenyl diselenide and water.

On the other hand, also diphenyl diselenide can be oxidised by H_2O_2 giving seleninic acid.[84] The formation of these less water soluble species was also suggested by the fact that a solid precipitate was observed in the NMR sample after the reaction study. Moreover, a signal at 1172.0 ppm was detected in the ^{77}Se NMR spectrum acquired at the end of the reaction, likely due to the presence of seleninic acid **8** (Fig. S32†).

Thus, to better clarify this behaviour and confirm the identity of the products, a more focused ^{1}H–^{77}Se HMBC NMR experiment was carried out. A mid-reaction sample from the oxidation study carried out on **1-CF$_3$** was diluted 1 : 1 in MeOD to completely dissolve the precipitate. The NMR analysis demonstrated the presence of *p*-trifluoromethyl seleninic acid **7** and 1,2-bis(4-(trifluoromethyl)phenyl)diselane **5**, respectively testified by the ^{77}Se signals detected at 447.9 and 1211.8 ppm (Fig. S29†). These findings are in agreement with previous observations by Wang and colleagues.[85] The authors studied the selenoxide elimination reaction in a simple model system by reacting a phenylalkylselenide with 2 equivalents of H_2O_2 in CD_3CN, observing the appearance of a signal at 1175.1 ppm in the ^{77}Se NMR spectrum, which is consistent with the presence of seleninic acid. Our results were further confirmed by ESI-MS experiments, as described in the following.

Investigation of the reaction mechanism by ESI-MS

Mass spectrometry, and ESI-MS in particular, can be used to identify the species in solution and complete the information obtained from NMR studies, even if few examples of its application to the chemistry and biochemistry of selenium are available.[39,86,87] In this study, mass spectra analysis was used as an independent technique for the identification and characterisation of the species involved in the transformation of the fluoxetine analogues and the compound identity was confirmed by collision-induced dissociation (CID) studies.

The monitoring of the reaction with H_2O_2 was carried out under the same experimental conditions (solvent, concentration, temperature) used to investigate the mechanistic details by NMR, working on independently prepared samples and according to the procedure reported in the Experimental section. Briefly, the reaction was carried out in water and time point samples were diluted 1 : 1000 in methanol before ESI-MS analysis. In analogy with the NMR protocol, the reaction of **1-H** was studied more in detail. In particular, the conversion of the starting material into the products was followed by sampling the reaction at the same time points used during the NMR experiments, and the two analytical techniques showed that the oxidation/elimination process was accomplished in a similar time frame (approximately 70 min, see Fig. S43†). Upon addition of H_2O_2, the signals corresponding to the selenoxide (m/z = 334) and cinnamylamine **6** (m/z = 162) were detected in the mass spectra obtained in positive ionisation mode. Moreover, MS analyses performed in negative ionisation mode highlighted the presence of the signal corresponding to seleninic acid **8** (m/z = 189, see Fig. S33–S36† for representative mass spectra), in agreement with the data reported by Wang and colleagues.[85]

Finally, MS analysis was also performed on the NMR samples used in the mechanistic study above described. Positive and negative ionisation mode MS spectra acquired on the

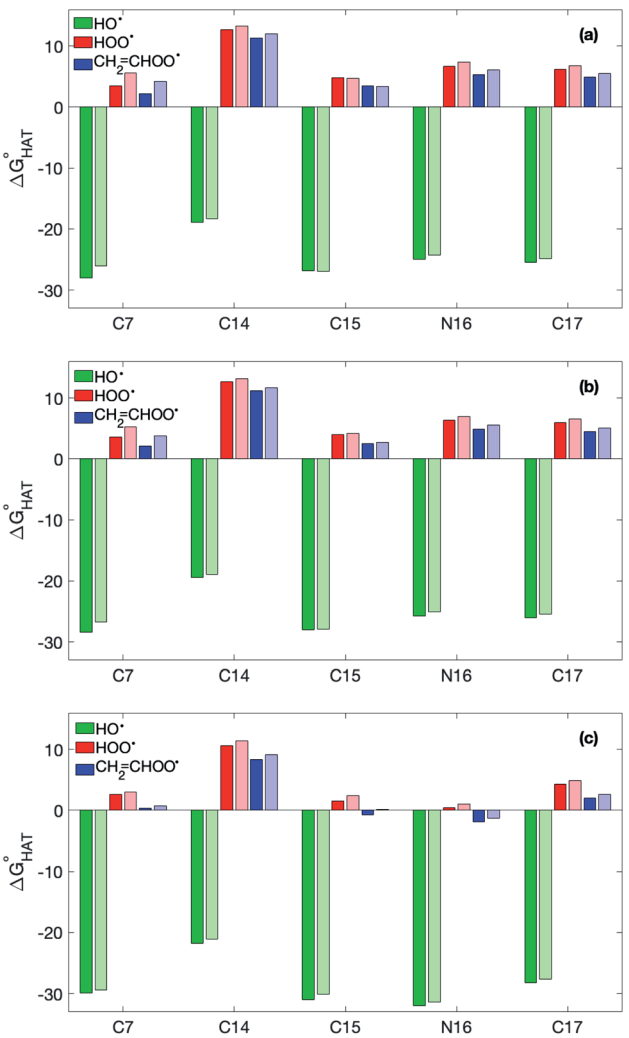

Fig. 3 ΔG°_{HAT} (kcal mol^{-1}) in the gas phase (a), in benzene (b), and in water (c) for the scavenging of HO$^{\bullet}$, HOO$^{\bullet}$ and CH$_2$=CHOO$^{\bullet}$ from non-aromatic sites of selenofluoxetine. Values for fluoxetine taken from Muraro *et al.*[17] are showed in a lighter shade for comparison. Level of theory: (SMD)-M06-2X/6-311+G(d,p)//M06-2X/6-31G(d).

Table 1 $\Delta G^{\ddagger}_{HAT}$ (kcal mol^{-1}) in the gas phase (a), in benzene (b), and in water (c) for the scavenging of HO$^{\bullet}$, from non-aromatic sites of selenofluoxetine. Level of theory: (SMD)-M06-2X/6-311+G(d,p)//M06-2X/6-31G(d)

HO$^{\bullet}$			
Site	Gas phase[a]	Benzene[a]	Water[a]
C7	2.8 (6.6)	3.8 (8.6)	4.1 (10.0)
C14	8.9 (7.5)	10.2 (8.9)	11.0 (9.5)
C15	4.6 (5.4)	5.3 (5.9)	3.0 (4.2)
N16	3.5 (3.7)	3.8 (4.0)	0.9 (0.8)
C17	6.1 (7.8)	4.1 (8.3)	6.4 (5.5)

[a] Values referring to the analogous sites of fluoxetine,[17] computed at the same level of theory, are reported in parentheses for comparison.

completely reacted sample (t = 24 h) diluted in methanol confirmed the presence of seleninic acid **8** (m/z = 189), diphenyl diselenide (m/z = 316) and cinnamylamine **6** (m/z = 162) as reaction products, that were identified using CID experiments (Fig. S37–S42†). A similar behaviour was observed for **1-CF$_3$**. Again, MS analysis on the sample reacted with H_2O_2 unambiguously confirmed the presence in solution of **6** (m/z = 162) and **7** (m/z = 255) as final products (Fig. S44 and S45†).

Mechanistic DFT analysis

The radical scavenging activity *via* HAT of fluoxetine has been recently investigated *in silico* by some of us.[17] HAT occurs from the non-aromatic sites C7, C14, C15, N16 and C17. We have considered the corresponding sites of selenofluoxetine (Scheme 1) and focused on the scavenging of HO$^{\bullet}$, which is the most reactive and electrophilic oxygen centred radical, of the peroxyl radical HOO$^{\bullet}$ and of CH$_2$=CHOO$^{\bullet}$, which mimics larger unsaturated peroxyl radicals. ΔG°_{HAT} values are shown in Fig. 3 and listed in Table S1.†

As reported for fluoxetine, selenofluoxetine is not selective for peroxyl radicals; in fact, all HATs from all the five sites to HOO$^{\bullet}$ and most HATs to CH$_2$=CHOO$^{\bullet}$ are endergonic in gas-phase as well as in solvent. Focusing on HAT to HO$^{\bullet}$, in gas phase, it is thermodynamically most favoured from C7, which is close to Se, and more favoured from C15 and N16 than from C14 and C17. ΔG°_{HAT} values become more negative when going from the gas to the condensed phase and with increasing solvent polarity. In benzene, the same trend of gas-phase is found; conversely, in water, HAT from the amino site is the most favoured, as found for fluoxetine. $\Delta G^{\ddagger}_{HAT}$ were computed for all five non-aromatic sites to HO$^{\bullet}$, *i.e.* those from C7, C14, C15, N16 and C17 and are reported in Table 1. In gas-phase, the lowest activation energy is computed for HAT from C7, which is also the most exergonic process. *i.e.* 2.8 kcal mol^{-1}. This value slightly increases in benzene where HAT from C7 becomes also less thermodynamically favoured process and decreases to 0.9 kcal mol^{-1} in water where ΔG°_{HAT} reaches the lowest negative value, *i.e.* −32.0 kcal mol^{-1}. Notably, in selenofluoxetine, HAT from all the five sites to HO$^{\bullet}$ is thermodynamically as well as kinetically more favoured than in fluoxetine, denoting a better radical scavenging potential.

The oxidation of the fluoxetine analogues by H_2O_2 was investigated *in silico* at ZORA-OLYP/TZ2P level of theory. In Fig. 4, the computed intermediates and transition states for selenofluoxetine are shown, while energy data are reported in Table S2.†

As can be seen from the energy profile shown in Fig. 5(a), in gas phase, the transition states are preceded and followed by the formation of a reactant complex (RCox) and a product complex (PCox), which are stabilised with respect to the free reactants and products, respectively. Upon reaction with H_2O_2, the selenide is oxidised to selenoxide. Since the attack of the peroxide may occur from two opposite sides, two paths are envisioned and two diastereoisomeric products form.

The oxidation occurring at selenium keeps the stereochemistry of C7 intact (*R*), therefore the two diastereoisomeric oxidised product differ only in the stereochemistry of selenium and are labelled *R*–*R* and *R*–*S* (Fig. 4). Despite sterically more hindered, there are no large differences in the energetics along the *R*–*R* path and *R*–*S* path, and the former is predicted to be slightly more stabilised. From the two products, *i.e.* *R*–*R*-Ox and *R*–*S*-Ox, elimination also occurs *via* two distinct paths with rather similar energetics, leading to the seleninic acid **7** and the alkene **6**. The energy profiles shown in Fig. 5(c) and (d) are those of **1-CF$_3$**. No large mechanistic and energy differences are computed between fluoxetine and **1-CF$_3$**, suggesting that small

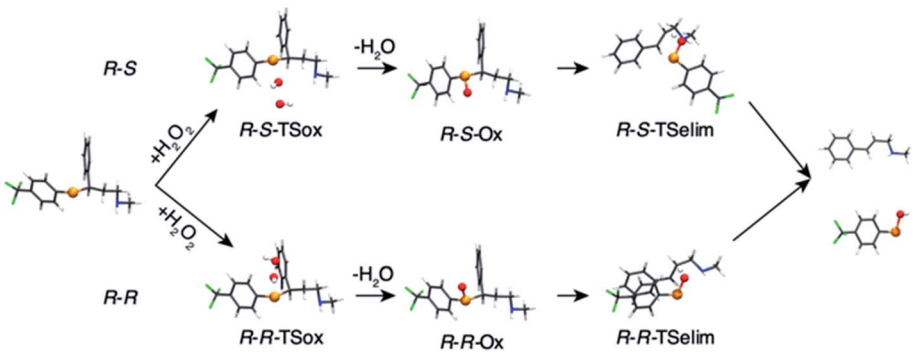

Fig. 4 Fully optimised geometries of intermediates and transition states of the oxidation of selenofluoxetine shown in Scheme 3 (R = H, R′ = CF$_3$). Reactant and product complexes are omitted for clarity. Level of theory: ZORA-OLYP/TZ2P.

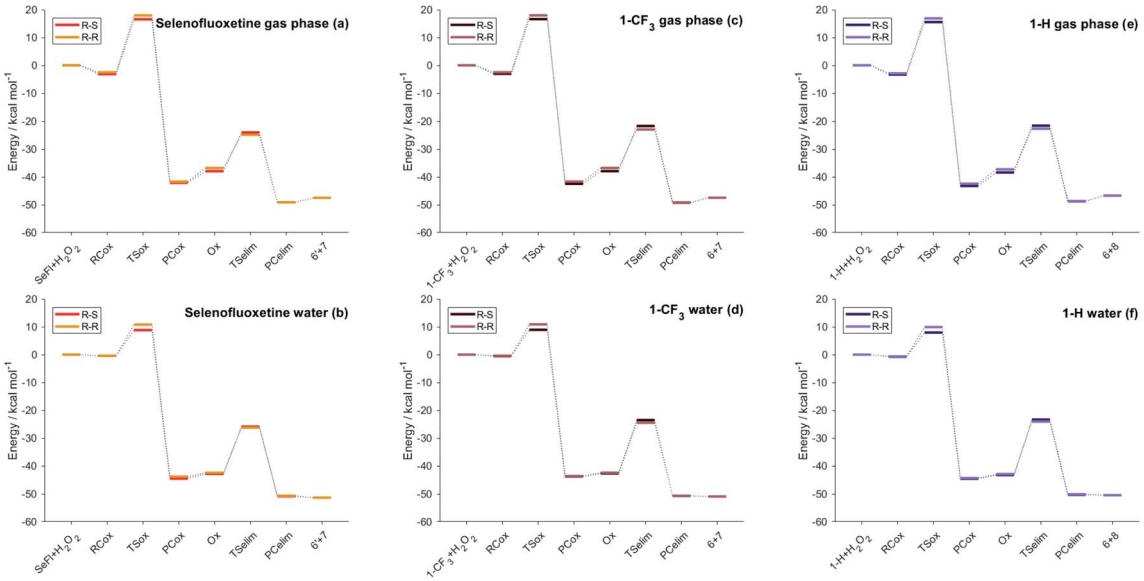

Fig. 5 Energies of the stationary points of the investigated reactions (Scheme 3) for different selenofluoxetine derivatives in the gas-phase (left column) and in water (right column). Level of theory: (COSMO)-ZORA-OLYP/TZ2P.

geometry modifications do not affect significantly the reactivity. Calculations have been carried out also for **1-H**. Considering the oxidation step, the barrier decreases when decreasing the electron-withdrawing character of the substituent on the phenyl ring R′, *i.e.* $\Delta E^{\ddagger}(R' = CF_3) > \Delta E^{\ddagger}(R' = H)$ (Table S2†). Conversely, in the elimination step, selenofluoxetine ($R' = CF_3$) has the lowest activation energy. The energy profiles of fluoxetine and **1-CF$_3$** have been recalculated also in solvent using the COSMO continuum approach for water. They are shown in Fig. 5(b) and (d). As reported for similar reactions,[88] we assist to the disappearance of the reactant and product complexes, which leads to a significant decrease of the activation energy for the oxidation step. Consequently, the highest barrier in water is the one computed for the elimination.

Conclusions

The results of our multi-approach experimental and theoretical investigation on the reaction of selenofluoxetine derivatives with H_2O_2 in water demonstrate that the substrates undergo an oxidation–elimination process, providing cinnamylamine and seleninic acid as final products. The model Se-based compounds here presented are closely related, from a structural point of view, to fluoxetine. Thus, they are expected to maintain the pharmacokinetic properties, such as CNS permeation, and biological activities of the original drug. Analogues of fluoxetine bearing tertiary amines were demonstrated to bind SERT with similar affinity.[89] Consequently, toxicological and medical research is prompted to further explore this aspect by probing the antidepressant potential of selenofluoxetine and its derivatives. Moreover, the studied organoselenides are novel *tandem antioxidants*, combining the radical scavenging properties of fluoxetine, which are mainly related to C7 and N16 sites, and serotonin-mediated redox activity, with the GPx-like reactivity, due to the presence of the selenium nucleus. In addition, the here reported reactions are also endowed with synthetic value, since the basis for a novel approach for the synthesis of cinnamylamine, a pharmacologically-relevant scaffold are presented. More in general, the here described procedure provides an efficient alternative, on the green chemistry side, for the preparation of the allylamine. The oxidation step can indeed be carried out in water, only requiring H_2O_2 and affording a quantitative conversion. Notably, the reaction is highly selective providing the *trans* products. Moreover, we verified that **1-CF$_3$** and **1-H** react following the same mechanism to give cinnamylamine. This prompted us to further investigate the oxidation–elimination reaction on other substrates in our ongoing investigation. Our perspective goal, supported by preliminary results, consists in probing the potential application of this methodology to a broader range of substrates for the production of unsaturated amines.

Conflicts of interest

There are no conflicts to declare.

Acknowledgements

This research was funded by the Università degli Studi di Padova, thanks to the P-DiSC (BIRD2018-UNIPD) project MAD^{3}S (Modelling Antioxidant Drugs: Design and Development of computer-aided molecular Systems); P. I. L. O. All the calculations were carried out on Galileo (CINECA: Casalecchio di Reno, Italy) thanks to the ISCRA Grant REBEL2 (REdox state role in Bio-inspired ELementary reactions 2), P. I.: L. O. L.O. contributed to this research as part of the scientific activity of the international multidisciplinary network 'SeS Redox and Catalysis'.

References

1 D. T. Wong, J. S. Horng, F. P. Bymaster, K. L. Hauser and B. B. Molloy, *Life Sci.*, 1974, **15**, 471–479.
2 D. T. Wong, K. W. Perry and F. P. Bymaster, *Nat. Rev. Drug Discovery*, 2005, **4**, 764–774.
3 J. A. Coleman and E. Gouaux, *Nat. Struct. Mol. Biol.*, 2018, **25**, 170–175.
4 M. G. Scordo, E. Spina, M.-L. Dahl, G. Gatti and E. Perucca, *Basic Clin. Pharmacol. Toxicol.*, 2005, **97**, 296–301.
5 C. Mancuso, E. Esposito, M. G. Morgese, F. Caraci, F. Tascedda, S. Merlo, C. Benatti, S. F. Spampinato, A. Munafò, G. M. Leggio, F. Nicoletti, N. Brunello, F. Drago, M. A. Sortino and A. Copani, *Front. Pharmacol.*, 2016, **7**, 389.
6 K. Manton, S. Volovik and A. Kulminski, *Curr. Alzheimer Res.*, 2004, **1**, 277–293.
7 P. R. Angelova and A. Y. Abramov, *FEBS Lett.*, 2018, **592**, 692–702.
8 K. Bisht, K. Sharma and M.-È. Tremblay, *Neurobiol. Stress*, 2018, **9**, 9–21.
9 M. C. W. Oswald, N. Garnham, S. T. Sweeney and M. Landgraf, *FEBS Lett.*, 2018, **592**, 679–691.
10 M. Bortoli, M. Dalla Tiezza, C. Muraro, C. Pavan, G. Ribaudo, A. Rodighiero, C. Tubaro, G. Zagotto and L. Orian, *Comput. Struct. Biotechnol. J.*, 2019, **17**, 311–318.
11 O. M. E. Abdel-Salam, S. M. Y. Morsy and A. A. Sleem, *EXCLI J.*, 2011, **10**, 290–302.
12 G. A. Behr, J. C. F. Moreira and B. N. Frey, *Oxid. Med. Cell. Longev.*, 2012, **2012**, 609421.
13 M. Herbet, M. Gawrońska-Grzywacz, M. Izdebska and I. Piątkowska-Chmiel, *Exp. Ther. Med.*, 2016, **12**, 3440–3444.
14 V. Caiaffo, B. D. R. Oliveira, F. B. de Sá and J. Evêncio Neto, *Pharmacol. Res. Perspect.*, 2016, **4**, e00231.
15 M. M. Safhi, H. M. Qumayri, A. U. M. Masmali, R. Siddiqui, M. F. Alam, G. Khan and T. Anwer, *Arch. Physiol. Biochem.*, 2019, **125**, 150–155.
16 N. Kolla, Z. Wei, J. S. Richardson and X.-M. Li, *J. Psychiatry Neurosci.*, 2005, **30**, 196–201.
17 C. Muraro, M. Dalla Tiezza, C. Pavan, G. Ribaudo, G. Zagotto and L. Orian, *Appl. Sci.*, 2019, **9**, 3631.
18 S. Sarikaya and I. Gulcin, *Curr. Bioact. Compd.*, 2013, **9**, 143–152.
19 O. Vašíček, A. Lojek and M. Číž, *J. Physiol. Biochem.*, 2020, **76**, 49–60.
20 A. Tutakhail, Q. A. Nazari, S. Khabil, A. Gardier and F. Coudore, *Life Sci.*, 2019, **232**, 116508.
21 O. Dalmizrak, K. Teralı, E. B. Asuquo, I. H. Ogus and N. Ozer, *Protein J.*, 2019, **38**, 515–524.
22 E. Byeon, J. C. Park, A. Hagiwara, J. Han and J.-S. Lee, *Aquat. Toxicol.*, 2020, **218**, 105337.
23 L. Orian and S. Toppo, *Free Radical Biol. Med.*, 2014, **66**, 65–74.
24 L. P. Wolters and L. Orian, *Curr. Org. Chem.*, 2015, **20**, 189–197.
25 M. D. Tiezza, G. Ribaudo and L. Orian, *Curr. Org. Chem.*, 2019, **23**, 1381–1402.
26 J. T. Rotruck, A. L. Pope, H. E. Ganther, A. B. Swanson, D. G. Hafeman and W. G. Hoekstra, *Science*, 1973, **179**, 588–590.
27 L. Orian, P. Mauri, A. Roveri, S. Toppo, L. Benazzi, V. Bosello-Travain, A. De Palma, M. Maiorino, G. Miotto, M. Zaccarin, A. Polimeno, L. Flohé and F. Ursini, *Free Radical Biol. Med.*, 2015, **87**, 1–14.
28 M. Bortoli, M. Torsello, F. M. Bickelhaupt and L. Orian, *ChemPhysChem*, 2017, **18**, 2990–2998.
29 L. Orian, G. Cozza, M. Maiorino, S. Toppo, F. Ursini, M. Maiorino, S. Toppo and F. Ursini, in *Glutathione, Series Oxidative stress and disease*, ed. L. Flohé, CRC Press, 2018, pp. 53–66.
30 M. Maiorino, V. Bosello-Travain, G. Cozza, G. Miotto, L. Orian, A. Roveri, S. Toppo, M. Zaccarin and F. Ursini, in *Selenium: its molecular biology and role in human health*, ed. Springer, 4th edn, 2016, pp. 223–234.
31 M. T. Zimmerman, C. A. Bayse, R. R. Ramoutar and J. L. Brumaghim, *J. Inorg. Biochem.*, 2015, **145**, 30–40.
32 A. Wendel, M. Fausel, H. Safayhi, G. Tiegs and R. Otter, *Biochem. Pharmacol.*, 1984, **33**, 3241–3245.
33 G. Mugesh, W. W. du Mont and H. Sies, *Chem. Rev.*, 2001, **101**, 2125–2179.
34 K. P. Bhabak and G. Mugesh, *Acc. Chem. Res.*, 2010, **43**, 1408–1419.
35 L. S. Galant, M. M. Braga, D. de Souza, A. F. de Bem, L. Sancineto, C. Santi and J. B. T. da Rocha, *Free Radical Res.*, 2017, **51**, 657–668.
36 A. F. de Bem, M. Farina, R. de L. Portella, C. W. Nogueira, T. C. P. Dinis, J. A. N. Laranjinha, L. M. Almeida and J. B. T. Rocha, *Atherosclerosis*, 2008, **201**, 92–100.
37 T. Posser, M. B. Moretto, A. L. Dafre, M. Farina, J. B. T. da Rocha, C. W. Nogueira, G. Zeni, J. dos S. Ferreira, R. B. Leal and J. L. Franco, *Chem.-Biol. Interact.*, 2006, **164**, 126–135.
38 G. Ghisleni, L. O. Porciúncula, H. Cimarosti, J. B. T. Rocha, C. G. Salbego and D. O. Souza, *Brain Res.*, 2003, **986**, 196–199.
39 G. Ribaudo, M. Bellanda, I. Menegazzo, L. P. Wolters, M. Bortoli, G. Ferrer-Sueta, G. Zagotto and L. Orian, *Chem.–Eur. J.*, 2017, **23**, 2405–2422.
40 C. Santi, S. Santoro, C. Tomassini, F. Pascolini, L. Testaferri and M. Tiecco, *Synlett*, 2009, **2009**, 743–746.
41 M. Tiecco, L. Testaferri, A. Temperini, F. Marini, L. Bagnoli and C. Santi, *Synth. Commun.*, 1999, **29**, 1773–1778.
42 M. Tiecco, L. Testaferri, A. Temperini, L. Bagnoli, F. Marini and C. Santi, *Synlett*, 2001, 1767–1771.
43 C. Santi, R. G. Jacob, B. Monti, L. Bagnoli, L. Sancineto and E. J. Lenardão, *Molecules*, 2016, **21**(11), 1482.
44 C. Santi, C. Tomassini and L. Sancineto, *Chimia*, 2017, **71**, 592–595.
45 C. Santi and L. Bagnoli, *Molecules*, 2017, **22**, 2124.
46 P. Frøyen and P. Juvvik, *Tetrahedron Lett.*, 1995, **36**, 9555–9558.
47 F. D. Lewis, G. D. Reddy, S. Schneider and M. Gahr, *J. Am. Chem. Soc.*, 1991, **113**, 3498–3506.
48 C. Chen, Y. Huang, Z. Zhang, X.-Q. Dong and X. Zhang, *Chem. Commun.*, 2017, **53**, 4612–4615.
49 Y. Zhao and D. G. Truhlar, *Theor. Chem. Acc.*, 2008, **120**, 215–241.
50 M. J. Frisch, G. W. Trucks, H. B. Schlegel, G. E. Scuseria, M. A. Robb, J. R. Cheeseman, G. Scalmani, V. Barone, G. A. Petersson, H. Nakatsuji, X. Li, M. Caricato,

A. V. Marenich, J. Bloino, B. G. Janesko, R. Gomperts, B. Mennucci, H. P. Hratchian, J. V. Ortiz, A. F. Izmaylov, J. L. Sonnenberg, D. Williams-Young, F. Ding, F. Lipparini, F. Egidi, J. Goings, B. Peng, A. Petrone, T. Henderson, D. Ranasinghe, V. G. Zakrzewski, J. Gao, N. Rega, G. Zheng, W. Liang, M. Hada, M. Ehara, K. Toyota, R. Fukuda, J. Hasegawa, M. Ishida, T. Nakajima, Y. Honda, O. Kitao, H. Nakai, T. Vreven, K. Throssell, J. A. Montgomery, J. A. Montgomery Jr, J. E. Peralta, F. Ogliaro, M. J. Bearpark, J. J. Heyd, E. N. Brothers, K. N. Kudin, V. N. Staroverov, T. A. Keith, R. Kobayashi, J. Normand, K. Raghavachari, A. P. Rendell, J. C. Burant, S. S. Iyengar, J. Tomasi, M. Cossi, J. M. Millam, M. Klene, C. Adamo, R. Cammi, J. W. Ochterski, R. L. Martin, K. Morokuma, O. Farkas, J. B. Foresman and D. J. Fox, *Gaussian 16, Revision B.01*, Gaussian, Inc., Wallingford, CT, 2016.

51 A. V. Marenich, C. J. Cramer and D. G. Truhlar, *J. Phys. Chem. B*, 2009, **113**, 6378–6396.

52 A. Galano, *Phys. Chem. Chem. Phys.*, 2011, **13**, 7178–7188.

53 G. te Velde, F. M. Bickelhaupt, E. J. Baerends, C. Fonseca Guerra, S. J. A. van Gisbergen, J. G. Snijders and T. Ziegler, *J. Comput. Chem.*, 2001, **22**, 931–967.

54 C. Fonseca Guerra, J. G. Snijders, G. te Velde and E. J. Baerends, *Theor. Chem. Acc.*, 1998, **99**, 391–403.

55 E. J. Baerends, T. Ziegler, A. J. Atkins, J. Autschbach, D. Bashford, O. Baseggio, A. Bérces, F. M. Bickelhaupt, C. Bo, P. M. Boerritger, L. Cavallo, C. Daul, D. P. Chong, D. V. Chulhai, L. Deng, R. M. Dickson, J. M. Dieterich, D. E. Ellis, M. van Faassen, A. Ghysels, A. Giammona, S. J. A. van Gisbergen, A. Goez, A. W. Götz, S. Gusarov, F. E. Harris, P. van den Hoek, Z. Hu, C. R. Jacob, H. Jacobsen, L. Jensen, L. Joubert, J. W. Kaminski, G. van Kessel, C. König, F. Kootstra, A. Kovalenko, M. Krykunov, E. van Lenthe, D. A. McCormack, A. Michalak, M. Mitoraj, S. M. Morton, J. Neugebauer, V. P. Nicu, L. Noodleman, V. P. Osinga, S. Patchkovskii, M. Pavanello, C. A. Peeples, P. H. T. Philipsen, D. Post, C. C. Pye, H. Ramanantoanina, P. Ramos, W. Ravenek, J. I. Rodríguez, P. Ros, R. Rüger, P. R. T. Schipper, D. Schlüns, H. van Schoot, G. Schreckenbach, J. S. Seldenthuis, M. Seth, J. G. Snijders, M. Solà, M. Stener, M. Swart, D. Swerhone, G. te Velde, V. Tognetti, P. Vernooijs, L. Versluis, L. Visscher, O. Visser, F. Wang, T. A. Wesolowski, E. M. van Wezenbeek, G. Wiesenekker, S. K. Wolff, T. K. Woo and A. L. Yakovlev, *ADF2018, SCM, Theoretical Chemistry*, Vrije Universiteit, Amsterdam, The Netherlands, 2018.

56 N. C. Handy and A. J. Cohen, *Mol. Phys.*, 2001, **99**, 403–412.

57 N. C. Handy and A. J. Cohen, *J. Chem. Phys.*, 2002, **116**, 5411–5418.

58 F. Zaccaria, L. P. Wolters, C. Fonseca Guerra and L. Orian, *J. Comput. Chem.*, 2016, **37**, 1672–1680.

59 M. Bortoli, L. P. Wolters, L. Orian and F. M. Bickelhaupt, *J. Chem. Theory Comput.*, 2016, **12**, 2752–2761.

60 E. Van Lenthe and E. J. Baerends, *J. Comput. Chem.*, 2003, **24**, 1142–1156.

61 E. van Lenthe, E. J. Baerends and J. G. Snijders, *J. Chem. Phys.*, 1993, **99**, 4597–4610.

62 E. van Lenthe, E. J. Baerends and J. G. Snijders, *J. Chem. Phys.*, 1994, **101**, 9783.

63 E. van Lenthe, J. G. Snijders and E. J. Baerends, *J. Chem. Phys.*, 1996, **105**, 6505–6516.

64 A. D. Becke, *J. Chem. Phys.*, 1988, **88**, 2547–2553.

65 M. Franchini, P. H. T. Philipsen and L. Visscher, *J. Comput. Chem.*, 2013, **34**, 1819–1827.

66 C. C. Pye and T. Ziegler, *Theor. Chem. Acc.*, 1999, **101**, 396–408.

67 A. Klamt and G. Schüürmann, *J. Chem. Soc., Perkin Trans. 2*, 1993, 799–805.

68 A. Klamt and V. Jonas, *J. Chem. Phys.*, 1996, **105**, 9972–9981.

69 M. Abid and A. Azam, *Bioorg. Med. Chem.*, 2005, **13**, 2213–2220.

70 K. Tóth, N. I. Wenzel, N. Chavain, Y. Wang, W. Friebolin, L. Maes, B. Pradines, M. Lanzer, V. Yardley, R. Brun, C. Herold-Mende, C. Biot and E. Davioud-Charvet, *J. Med. Chem.*, 2010, **53**, 3214–3226.

71 D. M. Perrine, N. R. Sabanayagam and K. J. Reynolds, *J. Chem. Educ.*, 1998, **75**, 1266.

72 J. C. Liou, S. S. Badsara, Y. T. Huang and C. F. Lee, *RSC Adv.*, 2014, **40**, 41237–41244.

73 A. Clemenceau, Q. Wang and J. Zhu, *Chem.–Eur. J.*, 2016, **22**, 18368–18372.

74 K. B. Sharpless, M. W. Young and R. F. Lauer, *Tetrahedron Lett.*, 1973, **14**, 1979–1982.

75 A. Krief, W. Dumont and A. F. De Mahieu, *Tetrahedron Lett.*, 1988, **29**, 3269–3272.

76 A. J. Waring and J. H. Zaidi, *J. Chem. Soc., Perkin Trans. 1*, 1985, 631.

77 H. J. Reich, S. Wollowitz, J. E. Trend, F. Chow and D. F. Wendelborn, *J. Org. Chem.*, 1978, **43**, 1697–1705.

78 K. L. Nuttall, *Ann. Clin. Lab. Sci.*, 2006, **36**, 409–420.

79 F. V. Singh and T. Wirth, *Catal. Sci. Technol.*, 2019, **9**, 1073–1091.

80 D. M. Freudendahl, S. Santoro, S. A. Shahzad, C. Santi and T. Wirth, *Angew. Chem., Int. Ed.*, 2009, **48**, 8409–8411.

81 B. Cerra, F. Mangiavacchi, C. Santi, A. M. Lozza and A. Gioiello, *React. Chem. Eng.*, 2017, **2**, 467–471.

82 L. Syper and J. Młochowski, *Tetrahedron*, 1987, **43**, 207–213.

83 J. Młochowski and L. Syper, in *Encyclopedia of Reagents for Organic Synthesis*, John Wiley & Sons, Ltd, Chichester, UK, 2001.

84 D. De Filippo and F. Momicchioli, *Tetrahedron*, 1969, **25**, 5733–5744.

85 L. Wang, K. Zhu, W. Cao, C. Sun, C. Lu and H. Xu, *Polym. Chem.*, 2019, **10**, 2039–2046.

86 A. Tepecik, Z. Altin and S. Erturan, *J. Autom. Methods Manage. Chem.*, 2008, **2008**, 1–6.

87 K. Bierla, S. Godin, R. Lobinski and J. Szpunar, *TrAC, Trends Anal. Chem.*, 2018, **104**, 87–94.

88 M. Bortoli, F. Zaccaria, M. Dalla Tiezza, M. Bruschi, C. Fonseca Guerra, F. M. Bickelhaupt and L. Orian, *Phys. Chem. Chem. Phys.*, 2018, **20**, 20874–20885.

89 J. Andersen, N. Stuhr-Hansen, L. G. Zachariassen, H. Koldsø, B. Schiøtt, K. Strømgaard and A. S. Kristensen, *Mol. Pharmacol.*, 2014, **85**, 703–714.